BUCKLING OF CONSTRAINED HYPER-ELASTIC BEAMS

CASPER H. L. BEENTJES

Mathematical Institute, University of Oxford, Oxford, UK

Abstract. The deformation of elastic beams in confined spaces has a wide range of applications in, inter alia, health care and the petroleum industry. Historically, the literature has mainly focussed on one-dimensional beams models [8, 9, 18]. This paper, however, follows a different approach, as we focus on two dimensional hyper-elastic beams confined by a set of parallel plates. Due to non-linearity of the governing equations, a finite element approach, implemented in FEniCS [13], is used to find numerical solutions to the model equations.

1. Introduction

Materials exhibiting considerable deformations under a load are of utmost importance in a wide range of engineering problems. Examples being the possibly disastrous failure of structures due to buckling or the use of a flexible endoscope in medical imaging. Historically attention has predominantly been focussed on geometrically unconstrained materials, i.e. materials for which the deformation is unbounded by external influence. However, as the endoscopy example shows, it might be necessary to consider the bending of material under external domain constraints, in this case the patients organ. Other examples of constrained material bending are the production of textured yarn by use of a stuffer-box [14], the treatment of arterial atherosclerosis by angioplasty and the use of drill-strings in the petroleum industry.

The investigation of bending materials has a long mathematical history and can be considered as one of the key problems in elasticity theory. One of the first rigorous mathematical treatments of a sub-problem in solid mechanics is that of the bending and buckling of unconstrained slender elastic beams, i.e. beams for which deformations are reversible, and goes all the way back to the work of Euler. Euler's treatise, which builds upon earlier work by members of the Bernoulli family, describes one-dimensional curves under (arbitrary) elastic deformations [12].

Extensions of Euler's elastica to constrained beams have been made in the past few decades settling certain uniqueness issues [16], deriving analytical results in special cases [8] and performing a numerical exploration of the bifurcation structure [9]. Although the formalism set out by Euler yields an acclaimed analytical theory of beam curves in the unconstrained case, it only describes slender beams and thus only covers a small subset of the problems encountered in our world. To treat materials which extend into more than one dimension, more general models in elasticity theory have to be used.

This paper explores parts of the bifurcation structure of geometrically constrained beams in two dimensions. As we are interested in the behaviour of elastic materials under possibly large deformations due to buckling we focus on a specific model in finite elasticity theory which

E-mail address: beentjes@maths.ox.ac.uk.

Date: Trinity term 2015.

2010 *Mathematics Subject Classification.* 74B20,74S05,74G60,74G65.

This text is based on a technical report for the Trinity 2015 Oxford Mathematics course Python in Scientific Computing lectured by Dr. P. Farrell.

describes hyper-elastic materials. The resulting model equations can become highly non-linear and they are thus studied by means of numerical simulations using the finite element method.

2. Geometrically constrained hyper-elastic beams

The cornerstone of modelling in solid mechanics is often the set of Newton's laws applied to the solid object under the continuum assumption. Newton's laws, however, leave the system under-determined and thus need to be accompanied by constitutive laws to close the system of equations. The most common set of constitutive equations used relates the strain, a measure for deformation, and stress in the material.

The simplest model uses a linear stress-strain relation, known as Hooke's law for solids which results in the theory of linear elasticity. We are, however, interested in the material behaviour under finite deformations and hence need to consider an extension of the linear theory known as finite strain theory. This theory accounts for both geometric non-linearity due to large deformations and non-linearity inherent to material properties.

2.1. **Hyper-elasticity.** Given a solid body $\Omega \subset \mathbb{R}^n$ we define a displacement field $\mathbf{u} : \Omega \to \mathbb{R}^n$ which will transform the undeformed body Ω to a deformed body $\Omega' \subset \mathbb{R}^n$. This displacement field can be decomposed into a rigid-body displacement, consisting of translations and reflections, and a deformation, which changes the body-shape. Using this decomposition, we define the deformation gradient tensor $\mathbf{F} = \mathbf{I} + \nabla \mathbf{u}$, which can be used in the linearisation of the true deformation.

Inherent to deformations one can define a potential energy functional due to the material deformations, the internal strain-energy density functional $W(\mathbf{F})$. For hyper-elastic materials it is assumed that from this potential energy a constitutive law for the stress in the material can be derived [15]. In doing so we could close the set of PDEs derived from Newtons law by combining them with these constitutive equations.

There is, however, an equivalent formulation of the equations which uses the principle of virtual work [15] and this lends itself very well to the method of finite elements (FEM) that will be used for numerical simulations. Given the internal strain energy we can construct the total potential energy Π of the solid body

$$\Pi(\mathbf{u}) = \int_\Omega W(\mathbf{F})\,\mathrm{d}\Omega + \int_\Omega \mathbf{u} \cdot \mathbf{f}\,\mathrm{d}\Omega + \int_{\partial\Omega} \mathbf{u} \cdot \mathbf{T}\,\mathrm{d}S, \tag{1}$$

here $\mathbf{f}, \mathbf{T}$ are the external body and surface force densities respectively and their integrals comprise the external contributions to the potential energy. For the rest of the paper we will consider the problem without any external force contributing to the potential energy.

Now, the principle of virtual work is applicable in the case of a stationary deformation, which is what we are interested in. It states that for any displacement field satisfying the correct boundary conditions (which are problem dependent) the potential energy will attain its minimum at the equilibrium solution.

By defining a function space U such that for all $\mathbf{u} \in U$ the boundary conditions are satisfied, we can consider the problem of finding an equilibrium solution to be equivalent to finding

$$\tilde{\mathbf{u}} = \arg\min_{\mathbf{u} \in U} \Pi(\mathbf{u}). \tag{2}$$

So far the internal strain energy has been discussed in its full generality, but in order to construct a more concrete model one needs to consider an explicit form of the strain energy.

Neo-Hookean model. A commonly used model for the strain energy is the Neo-Hookean model, which simplifies to Hooke's law for small displacements. Furthermore, it has the desirable property of being an objective functional, i.e. it is independent of an orthogonal transformation of coordinates such as rotations. As a result, it can only depend on invariants of the tensor $\mathbf{F}$ or tensors derived from this [15]. A frequently used form for two dimensions is given by

$$W = \frac{\mu}{2}\left(J^{-1}I_c - 2\right) + \frac{K}{2}(J-1)^2. \tag{3}$$

Here μ, K are the shear and bulk modulus respectively, which are material parameters. The tensor invariants are $I_c = \mathrm{Tr}(\mathbf{F}^T\mathbf{F})$ and $J = \det(\mathbf{F})$. The elastic moduli can be expressed in terms of the more widely used Poisson's ratio ν and Young's modulus E. In this paper we assume a plane stress formulation, and use [10] to find the bulk and shear modulus in the case of $\nu = 0.3$ and $E = 1$ GPa.

2.2. **Box-constraints.** Analogous to Pocheau & Roman [18] we consider the set-up depicted in Figure 1 of an hyper-elastic beam constrained by two parallel plates a distance Y apart. We can then control the separation of the plates Y and the displacement u of the endpoints of the beams. We thus impose a Dirichlet boundary condition on $\mathbf{u}$ at the ends of the beam. As noted by Pocheau & Roman this will only yield symmetric solutions around the center of the beam. To ensure this numerically (and to gain a factor two computationally) we can consider just a half beam with the appropriate boundary conditions enforcing a reflection symmetry. Due to friction effects and perturbations of the symmetry we can observe asymmetrical equilibrium solutions in nature, see for example [18], but this is outside the scope of this paper.

In performing a non-dimensionalisation we can choose to rescale by any natural length scale. The choice made in our formulation is to take L as the length scale, effectively enforcing $L = 1$. Subsequently, the beams are characterised by their slenderness ratio d/L.

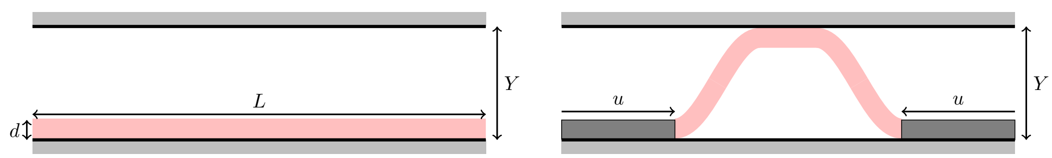

(A) Uncompressed beam

(B) Constrained buckled beam

FIGURE 1. Situation sketch of the hyper-elastic beam of length L and width d. The beam is constrained by two horizontal plates a distance Y apart and the endpoints are displaced by a distance u which can yield constrained buckled states which differ qualitatively from unconstrained observations.

Note that the experimental set-up for our two-dimensional problem would correspond to a one-dimensional beam problem with clamping boundary conditions at the endpoints, which is the specific set-up studied by Pocheau and Roman [18]. Results in the limit of infinitely slender beams, i.e. $d/L \ll 1$, are thus expected to agree with this simplified one-dimensional model. We are, however, not aware of any (numerical) results on the bifurcation structure for one-dimensional clamped-clamped boundary conditions.

3. NUMERICAL SIMULATION

3.1. **Finite elements using FEniCS.**

Variational form. The problem of finding a solution to (2) is solved by employing the finite element method (FEM). In order to use this method we first note that (2) implies that at the equilibrium we must have that the Gâteaux derivative of the energy functional vanishes for all admissible displacement fields, i.e.

$$\mathbf{0} = d\Pi(\tilde{\mathbf{u}}; \mathbf{v}) = \frac{d}{dh}\Pi(\tilde{\mathbf{u}} + h\mathbf{v})\Big|_{h=0}, \tag{4}$$

for all $\mathbf{v} \in U$. Under the assumption that $\Pi(\mathbf{u})$ is Fréchet differentiable, this gives us the following variational formulation of the problem

$$\text{find } \mathbf{u} \in U \text{ such that } G(\mathbf{u}; \mathbf{v}) = \mathbf{0} \quad \forall \mathbf{v} \in U, \tag{5}$$

where $G(\mathbf{u}; \mathbf{v}) = d\Pi(\mathbf{u}; \mathbf{v})$ is a semi-linear functional in the second argument, i.e. linear in $\mathbf{v}$.

This variational formulation can now be used to apply the FEM. In short, the infinite dimensional function space U is discretised, i.e. we take a finite dimensional subspace $U_h \subset U$ and solve (5) with U_h instead. As G is non-linear in the first argument we will have to use non-linear solver techniques such as Newton's method with some globalising strategy to solve the discretised system.

FEniCS and discretisation. The practical implementation of the FEM is done using FEniCS [13], an automated programming environment for solving differential equations using FEM, which we control using a Python interface.

We need to supply the variational form (5) and the FEM discretisation to be used. FEniCS then assembles the discretised system of FEM equations which can be solved using numerical linear algebra software, in this case we used the PETSc toolbox [3, 4, 7] in combination with the MUMPS package [1, 2]. To solve a constrained problem we use a variational inequality solver in PETSc which uses a reduced space active set method [5].

We discretise the domain using right triangles, see Figure 2 and use Lagrange elements, $\mathcal{P}_1$ or $\mathcal{P}_2$, to approximate the solution. Note that we anticipate the solution to be smooth as do not incorporate cracks or fractures in our model. As a consequence we should expect a smooth deformation field. Therefore we chose for the main results to use the higher order elements, $\mathcal{P}_2$ in this case, hoping to acquire a higher order of convergence, as is indicated in the following section.

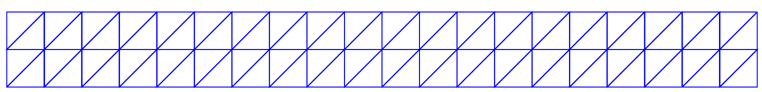

FIGURE 2. Structured right triangular mesh on a beam with slenderness ratio 0.1 constructed by FEniCS using 20 elements in the horizontal direction and 2 in the vertical direction.

3.2. **Convergence.** The convergence of the numerical discretisation was tested using the method of manufactured solutions (MMS) [17]. In a nutshell, having a numerical simulation, one would like to compare the results with known analytical solutions to check for a correct implementation and order of convergence. Exact solutions are generally not available for non-linear problems, but MMS allows us to tweak the problem so that we do have an analytical solution.

Suppose we are given a general equation

$$L(\mathbf{X}) = \mathbf{0}. \tag{6}$$

If we pick any $\tilde{\mathbf{X}}$ satisfying the correct boundary conditions, then we note that in general $L(\tilde{\mathbf{X}}) \neq \mathbf{0}$. From this, however, we can construct a related equation for which we do know the exact solution

$$L(\mathbf{X}) = \mathbf{b}, \tag{7}$$

where $\mathbf{b} = L(\tilde{\mathbf{X}})$ is now a source term. So we numerically solve the system $L(\mathbf{X}) - \mathbf{b} = \mathbf{0}$ instead of the original system. That way we can compare the numerical results with a known analytical solution $\tilde{\mathbf{X}}$ to find the convergence rates of the discretisation.

We choose our analytical test function to be one that lacks symmetry and is not a polynomial in one of the spatial variables, namely:

$$\mathbf{u}_{\mathrm{MMS}} = \left(A\left[1 - 2x^2 + 0.2\sin(2\pi x)\right], B\left[1 - \cos\left(\frac{2\pi x}{(1 + x(1-x))^4}\right)\right]\right)^T, \tag{8}$$

where A, B are such that the function satisfies the bounds set by the box. We test on a beam with slenderness ratio 0.1 and $Y = 0.2$. The results are depicted in Figure 3 and show that the theoretical convergence rates for Lagrange elements as found in [6] are achieved, indicating a correct implementation.

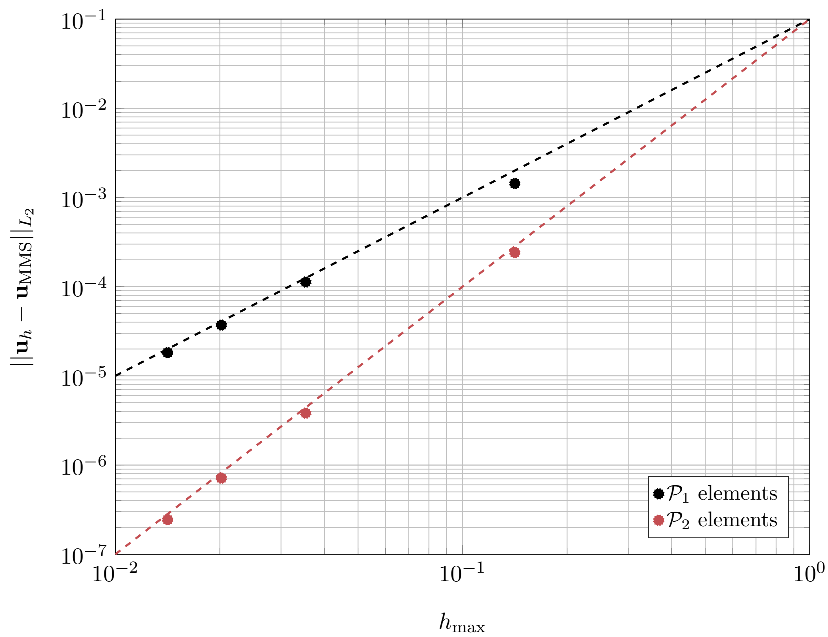

FIGURE 3. Convergence test using MMS. Shown is the convergence of the numerical solution $\mathbf{u}_h$ towards the test solution (8) in the L_2-norm for first and second order Lagrange elements as a function of the maximal edge length $h_{\max}$ of the elements. Dotted reference lines show the theoretical convergence rates as predicted in [6], $\mathcal{O}(h^2)$ for $\mathcal{P}_1$-elements and $\mathcal{O}(h^3)$ for $\mathcal{P}_2$-elements.

3.3. **Results.** Our model allows for the independent variation of both the horizontal compression u and vertical wall separation Y. We chose to look at the situation for fixed Y and compress the beam in the horizontal direction. Note that as we use a Newton solver to find the equilibrium solutions we need sufficiently good initial guesses to have our solver converge. In order to do so we employ a continuation scheme in u tracing out solutions for different horizontal loadings.

As observed by Domokos, Holmes & Royce in the case of a one-dimensional beam there is a clear distinction in the buckling behaviour of the beam depending on Y [8]. As sketched in Figure 1, the beam is likely to form a flat part on the top of the box. There appears to be a critical Y_c such that for $Y < Y_c$ this flat part can buckle, whereas for $Y > Y_c$ this will not happen. A possible explanation given in [18] is that the tension on the flat part becomes too small in the latter case to induce buckling. We observe a similar effect for extended hyper-elastic beams and will thus treat the results separately, although the status of an actual critical separation distance is merely a conjecture.

Large vertical separation Y. First we consider a beam with slenderness ratio 0.01. Note that as Y becomes very large the problem becomes effectively unconstrained by the upper wall. The only remaining constraint is the requirement that the vertical component of $\mathbf{u}$ is positive.

We expect therefore that there is a resemblance between the constrained beam with $Y > Y_c$ and the unconstrained beam buckling, where we only consider the upward buckling modes of the unconstrained beam. See Appendix A.1 for examples of the buckling modes occurring.

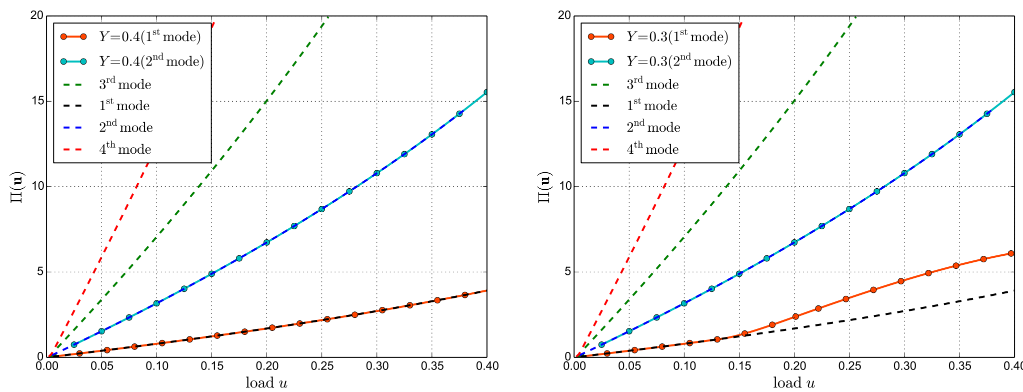

(A) $Y_c < Y = 0.04$

(B) $Y_c < Y = 0.03$

FIGURE 4. Potential energy $\Pi(\mathbf{u})$ as a function of the horizontal loading u for a hyper-elastic beam with slenderness ratio 0.01. The separation distance Y is in both cases large enough so that the beam behaves (nearly) as beam in constrained to the upper half-plane. The dashed lines indicate the energy in the unconstrained case. Note that every dot represents 5 continuation steps in u.

Indeed this is what is observed in Figure 4, where we can clearly see that the constrained energy functional remains very close to the unconstrained energy functional, indicating that the upper wall's effect on the beam is small. The separation in energy between the second and first mode remains too large to induce a transition via buckling as expected. Note however that there is a difference between the unconstrained case and our model problem, which appears as soon as the unconstrained beam curve hits the bounding walls, the beam has to conform to the box-bounds which as a result increases the energy potential of the beam due to a more unfavourable bending configuration.

Based on these observations we could think that the bifurcation structure of the beam is purely governed by unconstrained beam-buckling. However, an interesting side effect of the two-dimensionality of the beam is that it appears that the so-called zero solution, which only compresses in the horizontal direction without buckling, is not longer a valid solution. This might due to the Poisson effect (an effect which is absent in one-dimension), which makes the beam expand in the vertical direction upon compression in the horizontal direction. This will likely yield a perturbation on the local bifurcation structure close to the initial state. Although we have not checked this in full detail numerically, we expect that the higher order modes in this case emanate from the first mode.

Induced buckling by walls. As the separation distance Y decreases the constrained energy curve separates from the unconstrained beam curves for lower loading values. As noted in experiments [18] this can result in an extra bifurcation point which makes the solution buckle from the first mode to the second mode. In order for this to happen we need to find a smooth curve connecting the two solution branches. As this wall-induced buckling is observed in experiments we can expect that the second buckling mode becomes energetically more favourable at a certain critical loading value. A good indication on whether this type of buckling can occur is therefore the relative potential energy of the both modes. As can be seen from Figure 5, there is indeed a transition between $0.14 < Y < 0.2$ where the second mode becomes energetically more stable. This is merely an indicator of the actual wall-induced buckling as the problem of finding the connecting branch, however, proves to be very challenging. It seems to be very sensitive to correct initial guesses and finding a robust way to find the connecting branches remains a subject of further research.

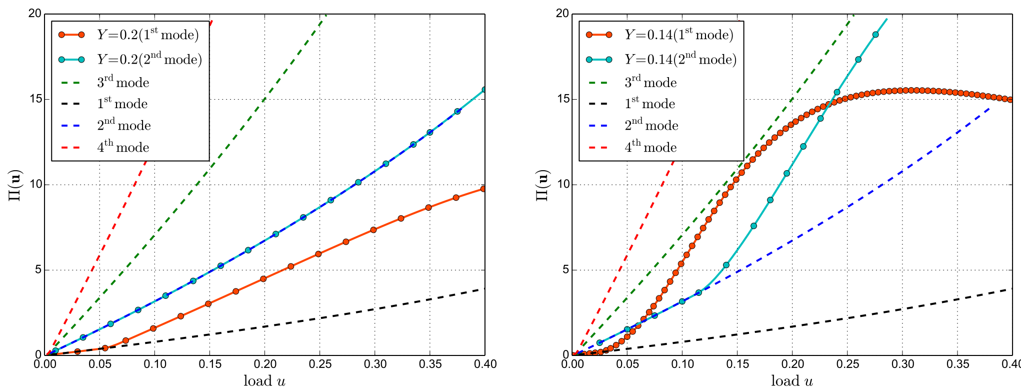

(A) $Y_c < Y = 0.2$

(B) $Y_c < Y = 0.14$

FIGURE 5. Potential energy $\Pi(\mathbf{u})$ as a function of the horizontal loading u for a hyper-elastic beam with slenderness ratio 0.01. The separation distance Y is not large, and thus the beam separates from the unconstrained curve for moderate values of compression. Note that every dot represents 5 continuation steps in u.

Formation of kinks. In the case of sufficiently thick beams we observed that the convergence using $\mathcal{P}_2$ elements would halt at a certain point of substantial loading. Switching to $\mathcal{P}_1$ elements to anticipate a possible loss of smoothness we found that the stagnation point coincided in most cases with the formation of kinks in the beam, see Figure 6.

The formation of these non-smooth parts in the beam deformation is the onset of a breakdown of our model equation as we can see that the beam almost starts to become self intersecting, which is of course physically prohibited. An extension of the model would have to be made which adds self-interaction in the energy potential.

4. CONCLUSION

In this paper we started a numerical exploration of the bifurcation structure of hyper-elastic beams confined in a box. The problem of solving the hyper-elastic equations subject to the box inequalities is numerically challenging and more work can certainly be done. Of special interest is the question whether we can find a robust way to find multiple solution branches if they exist and finding ways how to connect these branches in bifurcation points.

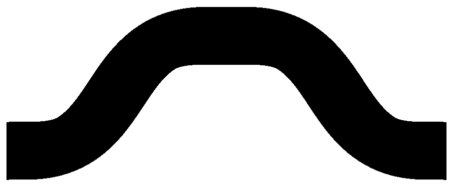

(A) $u = 0.12$

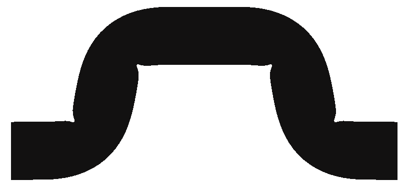

(B) $u = 0.16$

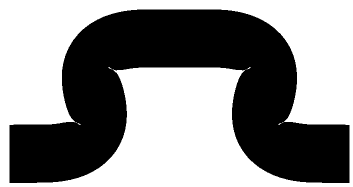

(C) $u = 0.2$

FIGURE 6. Formation of kinks in a thick beam with slenderness ratio 0.1. Deformed beam shapes generated using the calculated displacement field as found using $\mathcal{P}_1$ elements.

Although we did not focus on the slenderness ratio in this paper, it is interesting to see the influence of this parameter on the solution structure, as is shown by the appearance of kinks for thick beams. As thick beam theory is less well-developed this could be an interesting angle for further research.

Another obvious extension of the work carried out in this paper is making a full three dimensional simulation of beams or sheets constrained by boxes or tubular systems. This can open the door to a whole range of new phenomena such as helical buckling as studied for a one-dimensional Cosserat beam by Thompson et al. [19]. The implications of performing a numerical simulation of three dimensional hyper-elastic beams would be that direct solution methods for the linear systems arising in the process will turn computationally infeasible and thus (preconditioned) iterative solvers have to be employed.

As noted by Katz & Givli [11] the constraints in biological systems are often not rigid walls, but for example deformable artery walls. This would ask for an extension of the model by allowing the box constraints to deform as well. One idea might be to supplement the beams potential energy with a potential energy due to the deformation of the wall, thereby coupling the wall dynamics with that of the beam.

Appendix A. Appendix

A.1. **Beam shapes.** The beam shapes depicted in the following figures are acquired by using the actual numerically simulated displacement field on a beam with slenderness ratio 0.01. The displacement field can be used to map the original beam into the shapes depicted here.

1^{st} *mode.* The first buckling mode is shared by both the unconstrained and constrained problem as the displacement field is purely positive initially. As this is the state with the lowest potential energy, this will be the configuration observed in nature if no precautions are taken to find different solutions.

As noted in section 3.3, it is in the constrained case that the wall can induce an extra bifurcation linking the 2^{nd} mode and the first mode by letting the flat part buckle. The tension on the flat part could be too small to induce this buckling in which case the beam curve depicted in Figure 7(f) will be found.

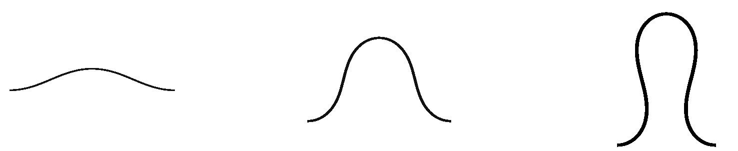

(A) small load (B) medium load (C) high load

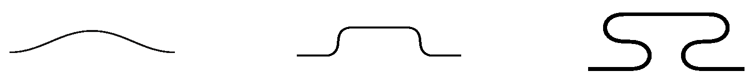

(D) small load (E) medium load (F) high load

Figure 7. First buckling mode for both the unconstrained ((a)-(c)) and constrained beam ((d)-(f)).

2^{nd} *mode.* Note that the second mode for the constrained cases coincides with what is often called the 3^{rd} mode for the unconstrained case. The second mode for the unconstrained case is not allowed by the box constraints as it has negative displacements.

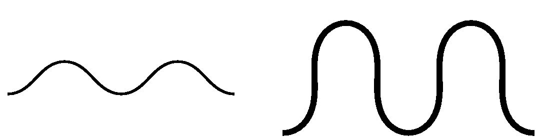

(A) small load (B) medium load (C) high load

(D) small load (E) medium load (F) high load

Figure 8. Second buckling mode for both the unconstrained ((a)-(c)) and constrained beam ((d)-(f)).

Higher modes are a trivial extension of the modes depicted here, simply involving more wrinkles due to buckling.

References

1. Amestoy, P., Duff, I., L'Excellent, J.-Y. & Koster, J. A Fully Asynchronous Multifrontal Solver Using Distributed Dynamic Scheduling. *SIAM Journal on Matrix Analysis and Applications* **23,** 15–41 (2001).
2. Amestoy, P., Guermouche, A, L'Excellent, J.-Y. & Pralet, S. Hybrid scheduling for the parallel solution of linear systems. *Parallel Computing* **32,** 136–156 (2006).
3. Balay, S., Gropp, W. D., McInnes, L. C. & Smith, B. F. *Efficient Management of Parallelism in Object Oriented Numerical Software Libraries* in *Modern Software Tools in Scientific Computing* (eds Arge, E, Bruaset, A. M. & Langtangen, H. P.) (Birkhäuser Press, 1997), 163–202.
4. Balay, S. *et al. PETSc Users Manual* tech. rep. ANL-95/11 - Revision 3.6 (Argonne National Laboratory, 2015).
5. Benson, S. J. & Munson, T. S. Flexible complementarity solvers for large-scale applications. *Optimization Methods and Software* **21,** 155–168 (2006).
6. Brenner, S. C. & Scott, R. *The Mathematical Theory of Finite Element Methods* 3rd ed. (Springer-Verlag New York, 2008).
7. Dalcin, L. D., Paz, R. R., Kler, P. A. & Cosimo, A. Parallel distributed computing using Python. *Advances in Water Resources* **34,** 1124–1139 (2011).
8. Domokos, G., Holmes, P. & Royce, B. Constrained euler buckling. *Journal of Nonlinear Science* **7,** 281–314 (1997).
9. Holmes, P., Domokos, G., Schmitt, J. & Szeberényi, I. Constrained Euler buckling: an interplay of computation and analysis. *Computer Methods in Applied Mechanics and Engineering* **170,** 175–207 (1999).
10. Jasluk, I, Chen, J & Thorpe, M. F. Elastic moduli of two dimensional materials with polygonal and elliptical holes. *Applied Mechanics Reviews* **47,** S18–S28 (1994).
11. Katz, S. & Givli, S. The post-buckling behavior of a beam constrained by springy walls. *Journal of the Mechanics and Physics of Solids* **78,** 443–466 (2015).
12. Levien, R. *The elastica: a mathematical history* tech. rep. UCB/EECS-2008-103 (EECS Department, University of California, Berkeley, 2008).
13. *Automated Solution of Differential Equations by the Finite Element Method* (eds Logg, A., Mardal, K.-A. & Wells, G.) (Springer-Verlag Berlin Heidelberg, 2012).
14. Lord, P. R. *Handbook of Yarn Production: Technology, Science and Economics* (CRC Press, 2003).
15. Ogden, R. W. *Non-Linear Elastic Deformations* (Dover Publications, 1984).
16. Pocheau, A. & Roman, B. Uniqueness of solutions for constrained Elastica. *Physica D: Nonlinear Phenomena* **192,** 161–186 (2004).
17. Roache, P. J. Code Verification by the Method of Manufactured Solutions. *Journal of Fluids Engineering* **124,** 4 (2002).
18. Roman, B. & Pocheau, A. Postbuckling of bilaterally constrained rectangular thin plates. *Journal of the Mechanics and Physics of Solids* **50,** 2379–2401 (2002).
19. Thompson, J. M. T., Silveira, M., van der Heijden, G. H. M. & Wiercigroch, M. Helical post-buckling of a rod in a cylinder: with applications to drill-strings. *Proceedings of the Royal Society A: Mathematical, Physical and Engineering Sciences* **468,** 1591–1614 (2012).